Published in final edited form as:
Nat Genet. 2011 February ; 43(2): 147–152. doi:10.1038/ng.752.

Disruption of mouse Slx4, a regulator of structure-specific nucleases, phenocopies Fanconi Anemia

Gerry P. Crossan[1], **Louise van der Weyden**[2], **Ivan V. Rosado**[1], **Frederic Langevin**[1], **Pierre-Henri L. Gaillard**[3], **Rebecca E McIntyre**[2], **Sanger Mouse Genetics Project**[2], **Ferdia Gallagher**[4], **Mikko I Kettunen**[4], **David Y Lewis**[4], **Kevin Brindle**[4], **Mark J Arends**[5], **David J Adams**[2], and **Ketan J Patel**[*,1,6]

[1]Medical Research Council, Laboratory of Molecular Biology, Hills Road, Cambridge CB2 0QH, UK.

[2]Wellcome Trust Sanger Institute, Wellcome Trust Genome Campus, Cambridge, UK

[3]Genome Instability and Carcinogenesis UPR3081 CNRS, Conventionné par l'Université d'Aix-Marseille 2, IGC, IMM 31 chemin Joseph Aiguier, 13402 Marseille, France

[4]Cancer Research UK, Cambridge Research Institute, Li Ka Shing Centre, Robinson Way, Cambridge CB2 0RE, UK

[5]Department of Pathology, Addenbrooke's Hospital, University of Cambridge, Cambridge, UK

[6]Department of Medicine, Addenbrooke's Hospital, University of Cambridge, Cambridge, UK

The evolutionarily conserved SLX4 protein, a key regulator of nucleases, is critical for the DNA damage response. SLX4 nuclease complexes mediate repair during replication and can also resolve Holliday junctions formed during homologous recombination. Here we describe the phenotype of the *Btbd12* knockout mouse, the murine orthologue of *SLX4*, which recapitulates many key features of the human genetic illness Fanconi Anaemia (FA). *Btbd12* deficient animals are born at sub-Mendelian ratios, have greatly reduced fertility, are developmentally compromised, and prone to blood cytopenias. *Btbd12*$^{-/-}$ cells prematurely senesce, spontaneously accumulate damaged chromosomes and are particularly sensitive to DNA crosslinking agents. Genetic complementation reveals a crucial requirement for Btbd12/Slx4 to interact with the structure specific endonuclease Xpf-Ercc1 to promote crosslink repair. The *Btbd12* knockout mouse therefore establishes a disease model for FA and genetically links a regulator of nuclease incision complexes to the FA DNA crosslink repair pathway.

Repairing most forms of genome damage requires DNA cleavage, a process catalysed by structure specific endonucleases (SSE)[1,2]. These enzymes are only recruited to chromatin when they are required for DNA repair. An important regulator of SSEs is the highly conserved SLX4/BTBD12 protein[2-4]. Previous studies suggest that SLX4 is likely to exert its function in genome stability by interacting and regulating three different SSEs through distinct and non-overlapping regions [5-7]. At the N-terminus SLX4 interacts with the XPF-ERCC1 nuclease complex, a central region binds MUS81-EME1 and a distinct C-terminal

*Corresponding author.

Author Contributions KJP and GPC designed the study, experiments and wrote the paper. GPC performed the majority of the experiments presented. DJA helped in design of the experiments. MJA analyzed histological samples and provided useful discussion. LvdW managed colony, weighed and performed necropsies on mice at WTSI. IVR analysed Fanconi pathway activation. FL assisted in analysis of developmental abnormalities. PHLG helped in the design of some experiments. REMcI performed micronucleus assay. SMGP performed mouse phenotype pipeline analysis. FG, MK, DL and KB performed imaging studies.

Europe PMC Funders Author Manuscripts

domain binds SLX1. In addition to interacting with SSEs, SLX4 also interacts with the mismatch repair recognition complex MSH2-MSH3 and also with components of the telomere shelterin complex, TRF-RAP1[6]. Moreover yeast and human SLX4 are phosphorylated by Tel1 and ATR kinases respectively [8,9] thereby connecting SLX4 to a replication-coupled DNA damage response network. Here we generate and analyse a mouse knockout of *Btbd12*, the murine orthologue of SLX4. These mice bear a striking resemblance to the phenotype of Fanconi Anaemia in humans, providing a long sought after animal model for this genetic illness.

Disruption of the murine *Btbd12* locus and creation of knockout mice, carrying the *Btbd12*$^{tm1a(EUCOMM)Wtsi}$ allele, were generated in the C57BL/6NTac background by the EUCOMM consortium, phenotyping was conducted at both our facility and the Wellcome Trust Sanger Institute. The structure of targeting construct, determination of site-specific integration, neomycin copy number and germline transmission of the allele was confirmed by PCR (Supplementary Fig 1 a-d). We confirmed that homozygous animals do not express detectable *Btbd12* mRNA by qPCR (Supplementary Fig 1e).

Btbd12$^{-/-}$ mice were born from heterozygous intercrosses, however the frequency of homozygotes was 11%, below the expected Mendelian ratio (χ^2-test; p=0.0007, Supplementary Table 1). From birth *Btbd12*$^{-/-}$ mice displayed marked growth retardation compared to wild type and heterozygous littermates (Figure 1a, b and Supplementary Fig 1f). Slx4 is highly expressed in the gonads (Supplementary Fig 2a), and unsurprisingly both male and female *Btbd12*$^{-/-}$ mice displayed a dramatic reduction in fertility due to gonad dysfunction. The fertility of a cohort of male and female homozygous animals crossed with wild-type animals was severely reduced producing only 9 pups, compared to a cohort of heterozygous littermate intercrosses producing 521 pups (Supplementary Table 2).

The SLX4-SLX1 heterodimer is a putative Holliday junction resolvase [5,6], predicting a role for *Slx4* in meiotic recombination. Histologically, *Btbd12*$^{-/-}$ ovaries at 16 weeks showed a complete absence of oocytes with no evidence of normal follicular maturation or corpora lutea(Fig 1c). Examination of 8-week-old testes revealed many tubules with evidence of defective spermatogenesis (Supplementary Fig 2 b). However at 16 weeks the majority of tubules lacked any spermatogenesis containing only Sertoli cells with the epididymis being devoid of spermatozoa (Fig 1c). The combination of the histological features and functional aspects of reduced fertility in *Btbd12*$^{-/-}$ mice resembles *Fanca*$^{-/-}$, *Fancl*$^{-/-}$ and *Ercc1*$^{-/-}$ mice, in all these instances infertility is the result of primordial germ cell failure (Fig 1c)[10-13]. The fact that limited spermatogenesis does occur and that young homozygous males and females can produce viable offspring indicates that meiosis can occur in *Btbd12*$^{-/-}$ mice. However it is noteworthy that in 8-week-old *Btbd12*$^{-/-}$ testes we observed multinucleated tetrads, and cells with multipolar spindles and an increased number of apoptotic bodies (Supplementary Fig 3a and b). These abnormalities could be consistent with defective meiosis.

A significant proportion of *Btbd12* deficient mice died soon after birth (Fig 2a). This subpopulation was severely runted and invariably associated with developmental defects resulting in domed skulls (Fig 2b, p=0.006, Fisher's exact test). High-resolution X-ray computed tomography images of a representative *Btbd12*$^{-/-}$ animal in Figure 2c show that the skull is enlarged and abnormal in shape. MRI imaging revealed gross cerebral enlargement due to a hydrocephalus causing cortical thinning, with compression of the brainstem and cerebellar structures. Histological analysis of the brain of hydrocephalic mice revealed extreme dilation of the lateral ventricles with rupture of the 3rd ventricle and of the cerebral cortex (Fig 2d). The MRI revealed that the 4th ventricle was spared suggesting an obstructive cause for the hydrocephalus (Fig 2e). *Btbd12*$^{-/-}$ mice also exhibited an increased

prevalence of ocular abnormalities compared to control littermates (Fig 2f, Supplementary Fig 4). MRI of a representative *Btbd12*$^{-/-}$ mouse with unilateral anophthalmia is shown in Figure 2g, revealing absence of the globe and no visible optic nerve. A significant proportion of *Btbd12*$^{-/-}$ mice also displayed a range of more subtle ocular abnormalities. (Fig 2h and Supplementary Fig 4a-c).

We assessed the haematological status of *Btbd12*$^{-/-}$ mice measuring red blood cells, white blood cells, and platelets (Fig 3 a-c). The mean white blood cell count is lower in *Btbd12* deficient animals compared with the control group. More significantly, a proportion of *Btbd12*$^{-/-}$ animals have very low levels of platelets. In most instances the same animals had deficiencies of both blood constituents. In order to gain insight into this haematological dysfunction we examined the capacity of blood progenitors to differentiate by colony forming assays. As can be seen in Figure 3d-e, bone marrow progenitors obtained from *Btbd12*$^{-/-}$ animals show a markedly reduced number of colony forming units for both myeloid and pre-B cell lymphoid lineages. Finally, we tested whether there was evidence of spontaneous genomic instability in the haematopoietic compartment. Figure 3f shows that the prevalence of micronucleated normochromic erythrocytes is elevated 2.5-fold in *Btbd12*$^{-/-}$ (Supplementary Fig 5)[14]. This indicates that spontaneous chromosomal instability occurs in the haematopoietic compartment of *Btbd12*$^{-/-}$ animals.

Primary *Btbd12*$^{-/-}$ MEF cultures rapidly ceased proliferating *in vitro* under normoxic conditions illustrated in Figure 4a. The reason for premature replicative senescence appears to be the accumulation of damaged chromosomes (Fig 4b and c). We observed chromosomal aberrations ranging from chromatid breaks to complex radial structures in metaphases produced from third passage *Btbd12*$^{-/-}$ MEFs (data not shown). We tested if chromosomal aberrations could be induced following treatment with DNA crosslinking agents. When *Btbd12*$^{-/-}$ transformed MEFs (tMEFs) were exposed to mitomycin C (MMC) for 48 hrs a dramatic increase in broken and radial chromosomes was observed. This induction of chromosomal aberrations was comparable to the increase observed in *Fanca*$^{-/-}$ tMEFs and significantly greater than in the *Btbd12*$^{+/+}$ congenic tMEF cell line (Fig 4d and e, Supplementary Fig 6 a-c).

We then asked if the *Btbd12*$^{-/-}$ tMEF cell lines were sensitive to exogenous DNA damage. siRNA knockdown of *SLX4* in human cancer cell lines results in hypersensitivity to the alkylating agent methylmethane sulfonate (MMS)[5-7], topoisomerase inhibitor camptothecin (CPT)[5,6] and crosslinking agents cisplatinum and MMC[7]. We therefore tested our cell lines for increased sensitivity to these DNA damaging agents as well as to γ and UV irradiation. It is clear from the data in Figure 5a and b that *Btbd12*$^{-/-}$ tMEFs were particularly sensitive to the two different DNA crosslinking agents – MMC and cisplatinum. However no hypersensitivity to MMS, γ, or UV irradiation was detected (Fig 5 c-e). *Btbd12*$^{-/-}$ tMEFs were slightly sensitive to CPT (Fig 5 f). Finally we compared the *Btbd12*$^{-/-}$ tMEFs to *Ercc1*$^{-/-}$, *Fanca*$^{-/-}$ and *Fancc*$^{-/-}$ SV40 tMEFs for sensitivity to MMC and UV irradiation. The data in Figure 5 g clearly shows that in a back-to-back comparison all strains are sensitive to MMC, with the *Btbd12*$^{-/-}$ and *Ercc1*$^{-/-}$ knockouts being the most sensitive. In contrast only the *Ercc1*$^{-/-}$ tMEFs are sensitive to UV irradiation (Fig 5 h). *Btbd12*$^{-/-}$ cells are competent in the monoubiquitination, recruitment to chromatin, and focus formation of Fancd2 (Supplementary Fig 7 a-c). Cumulatively *Btbd12*$^{-/-}$ cell lines show spontaneous and mutagen-induced genomic instability akin to FA patient cell lines as well as cells obtained from mouse FA gene knockouts [15].

Previous studies have already shown that all three SLX4 interacting SSEs (XPF-ERCC1, MUS81-EME1, and SLX1) participate in crosslink repair [2,16,17]. We therefore set out to establish whether some or all of these interactions contribute to crosslink repair. We made

two Slx4 deletion constructs that were predicted to disrupt key interactions with the respective SSE (Fig 6a). *Slx4*Δ*Ercc1* deletes the N terminal 498 residues predicted to disrupt the interaction with Xpf-Ercc1[5,6], whereas *Slx4*Δ*Slx1* deletes C terminal 148 residues predicted to disrupt the interaction with Slx1. The interactions of these Slx4 truncations with each SSE were tested using the mammalian-2-hybrid system and the expected interactions were lost (Supplementary Fig 8a).

Btbd12$^{-/-}$ tMEF cells lines stably expressing tagged Slx4, or Slx4 truncations were generated. Western blot analysis showed that all cDNA constructs directed the expression of nuclear proteins of the expected molecular size and with the predicted interactions with either Ercc1 or Mus81 (Fig 6b and Supplementary Fig 8b). The full-length cDNA and *Slx4*Δ*Slx1* complemented the *Btbd12*$^{-/-}$ tMEF hypersensitivity to MMC (Fig 6c). In contrast the *Slx4*Δ*Ercc1* did not complement this defect indicating that the interaction between SLX4 and the heterodimeric endonuclease Xpf-Ercc1 is crucial for crosslink repair. XPF-ERCC1 exerts its action when localised to chromatin, and in *Btbd12*$^{+/+}$ cell extract a proportion of the ERCC1 subcomponent can be detected constitutively bound to chromatin (Fig 6d top). In contrast in the *Btbd12*$^{-/-}$ cells the levels of Ercc1 on chromatin were barely detectable (Fig 6d top). Following exposure to MMC or UV (Figure 6d bottom and Supplementary Fig 8c) there is an increase in Ercc1 in the chromatin fraction in *Btbd12*$^{+/+}$ cells, whilst *Btbd12*$^{-/-}$ MMC damaged cells have a defect in the accumulation of Ercc1 in chromatin.

Btbd12 knockout mice recapitulate many key features associated with human FA, including the development of blood cytopenias and diverse developmental defects. The eye, brain, skeletal defects (Supplementary Fig 9) and abnormal glucose metabolism (Supplementary Fig 10) that we describe in *Btbd12*$^{-/-}$ mice have all been reported in human FA[18]. We note that the phenotype of Btbd12 knockout mouse differs from those carrying knockouts of each of these individual SSEs (Supplementary Table 3). The Slx4-Slx1 complex is a putative Holliday junction resolvase and its inactivation may in part explain the loss of fertility due to defective meiosis. However the infertility reported here closely resembles the infertility reported in FA and Ercc1 knockout mice which is due to primordial germ cell failure[10,12,13,19].

We show here that the interaction between Slx4 and Ercc1 is required for crosslink repair, it is therefore not a surprise that there are overlaps but importantly also significant differences between the phenotypes of the *Btbd12* and *Ercc1* knockout mice. For instance the pattern of sterility, bone marrow dysfunction and marked crosslinker sensitivity at the cellular level are shared aspects to both knockouts. The key cellular difference between *Ercc1* and *Btbd12* is the additional hypersensitivity of *Ercc1*$^{-/-}$ cells to UV[20]. *Ercc1* deficient mice display a severe phenotype with the majority of animals succumbing to hepatic failure before weaning [21,20,22]. This is in contrast with *Btbd12*$^{-/-}$ mice that do not show abnormal liver or renal function at 15 weeks (Supplementary Fig 11). Progressive neurodegeneration occurs in Ercc1 models but at 12 weeks *Btbd12*$^{-/-}$ had not developed neurodegenerative changes (Supplementary Fig 12)[23,24]. The striking parallels that we draw between *Btbd12/Slx4* knockout mice and human Fanconi anaemia make this gene a strong candidate for mutations in undesignated FA complementation groups. In a convergence with our mouse genetic study biallelic mutations in *SLX4* have now been identified in a potential new FA complementation group FANCP.

Online Methods

Targeting of ES cells and animal husbandry

Heterozygous mice carrying a targeted *Btbd12*$^{tm1a(EUCOMM)Wtsi}$ allele, were obtained from the EUCOMM consortium. ES cell lines were selected on neomycin and screened by long range PCR. Correct integration of the 5′ arm was confirmed using an oligo external to the targeting vector, V0RW_18_H08_gf2 , and an oligo inside the drug resistance cassette, LAR3_1, all oligonucleotide sequences are provided in Supplementary Table 4. The 3′ arm was screened using an oligo external to the targeting vector, V0RW_18_H08_gr1, and an oligo inside the drug resistance cassette RAF5. In both cases the amplicon was verified by sequencing. The presence of the loxP site was confirmed by sequencing using the LR oligo. Three positive ES cell lines were obtained. Two independent ES cell clones were injected. Targeted alleles from both clones were transmitted through the germline establishing independent colonies of mice on a C57BL/6N background that were phenotyped in parallel. Mice from these colonies were found to be indistinguishable excluding the possibility of linked mutations. To confirm a single integration event DNA from *Btbd12*$^{+/+}$, *Btbd12*$^{+/-}$ *and Btbd12*$^{-/-}$ animals was used as template for neomycin copy number counting using Neo and Dot1L primers (Supplementary Table 4). To genotype animals ear biopsies were obtained, DNA extracted, and used as the template for PCR using the following oligos GSlx4f, GSlx4r; GSlx4SAr. All animals were maintained in specific pathogen-free conditions. In individual experiments all mice were matched for age and gender. All animal experiments undertaken in this study were done so with the approval of the UK Home Office.

Preparation of Murine Embryonic Fibroblasts (MEFs)

Btbd12 heterozygous animals were time mated and humanely sacrificed at E13.5. Primary MEF cultures were obtained as described previously. When the cells reached confluence they were trypsinized and replated, this was considered passage 1.

Replicative senescence

6×10^5 MEFs from individual embryos were plated in a 6 well plate in triplicate. For subsequent passages cells were seeded at 1.2×10^5. Cells were passaged every 72 hours and enumerated using trypan blue exclusion counting 100 images using a ViCell XR (Beckman Coulter).

Cytogenetic analysis

was performed as described as previously. Briefly, tMEFs were treated with 50nM MMC in media for 48 hours prior to harvesting. tMEFs or passage 3 primary MEF were treated as described previously.

Transformation of MEFs

pBABE-SV40Puro virus was produced in PLAT-E cells (Cell Biolabs). 48h following transfection the media containing retrovirus was collected, and 0.22 micron filtered. The infection mix consisted of 50% retrovirus and 50% complete media supplemented with 4ug/mL polybrene. Clones were selected for 10 days using 3.5μg/mL puromycin.

Complementation

Truncations of *Btbd12* cDNA constructs were amplified with a N-terminal 2×FLAG tag from murine cDNA IMAGE clone (30534878). They were sequenced and cloned into pExpress and subsequently into pLoxBSR. The plasmids were transected into tMEF using Lipofectamine LTX (Invitrogen) following the manufacturers instructions. Positive clones

were selected using 10μg/mL blasticidin and screened for expression by western blot. Selection was maintained on positive clones.

DNA damage sensitivity assays

500 cells were plated per well of a 96-well plate, 12 hours later DNA damaging agent was added. Following 10 days MTS reagent (Promega) was added for 2 hours and absorbance was measured at 492nm. Each point represents the mean of three independent experiments each carried out in triplicate.

Sub-fractionation and Immunoblot

Sub-fractionation was achieved using a cellular subfraction kit (Thermo Scientific) according to manufacturer's instructions. Antibodies used were ERCC1 D-10 (Santa Cruz) at 1:100, Mus81F-20 (Santa Cruz) at 1:1000, FLAG M2 (Sigma) 1:2000, Histone 1 (Santa Cruz) 1:2000, PCNA (Sigma) 1:1000, β-tubulin (Abcam) 1:1000, FANCD2 antisera described previously[25].

Immunofluoresence

Cells were fixed with 3% paraformaldehyde for 15 minutes, and permeabilized with 0.2% Triton-X100 in PBS for 10 minutes. Cells were processed as described previously. Mouse FLAG M2 (Sigma) was used at a concentration of 1:500. Secondary Goat anti-Rabbit Alexafluor-555 (Invitrogen) was used at 1:500. Preparations for FANCD2 foci were pre-extracted with 0.1% Triton-X100 for 2 minute prior to treatment as above, rabbit anti-hFANCD2 antibodies have been described previously and were used at 1μg/mL. Imaging was performed on Nikon C1-si confocal microscope.

Mamalian-2-hybrid

was conducted as described previously[25]. The murine cDNA of each gene was amplified from the IMAGE clone *Btbd12* (30534878), *Slx1* (40130991), *Mus81* (5038349), and *Xpf* (4911382) cloned into the mammalian-2-hybrid vector and sequenced. Firefly and Renilla luciferase were assayed using Dual-Luciferase Reporter (Promega) following the manufacturer's protocol.

Micronucleus assay

flow cytometric analysis was performed as described previously[14].

Peripheral Blood Counts

Blood was collected in ETDA microvette tubes (Startedt) and analyzed on a VetABC analyzer.

Hematopoietic CFU Assays

were performed using bone marrow harvested from the femur. Cells were enumerated and equal numbers seeded in Methocult GF M3434 (Stem Cell Technologies) for myeloid lineages following the manufacturer's instructions. Pre-B cell CFU assays were performed using Methocult M3630 (Stem Cell Technologies) following the manufacturer's instructions.

Magnetic resonance imaging

Magnetic resonance imaging (MRI) data were collected from formalin-fixed whole animals and heads at 9.4 T using an Oxford Instruments, a Varian INOVA console and a quadrature ^{1}H-tuned volume coil (Varian Inc., Palo Alto, USA). Animals were administered

Europe PMC Funders Author Manuscripts

with 10mL/kg gadoteridol (ProHance®, Bracco diagnostics Inc., UK) by intraperitoneal injection 30 min prior to administration of a lethal dose of anaesthesia; animals were formalin-fixed and in some cases the heads were detached prior to imaging. Axial and sagittal proton (^{1}H) images were acquired from 1 mm slices using T_1-weighted gradient echo (repetition time 300 ms, echo time 2.7 ms) and T_2-weighted spin echo (repetition time 3000 ms, echo time 30 ms) pulse sequences. The field of view was 5.12 × 2.56 cm and data were collected into 512 × 256 matrices producing a 100 μm in-plane resolution. An additional three-dimensional 100 μm resolution isotropic data set was collected for the formalin-fixed heads using a gradient echo pulse sequence (field of view 4.80 × 1.92 × 1.92 cm, data matrix 480 × 192 × 192, repetition time 50 ms, echo time 2.7 ms).

X-ray Computed Tomography

Computed tomography was performed using a microtomography system (NanoPET™-CT, Mediso Ltd., Hungary). Images were obtained by helical acquisition using an exposure of 65 kVp, 123 μA and 1100 ms and a 78 μm resolution isotropic data set was acquired. Images were reconstructed using a modified cone beam filtered-back projection method using a RamLak filter and displayed as maximum intensity projections (InVivoScope® 1.41, Bioscan Inc., Washington DC).

Histology

Tissue samples were fixed in 10% NBF, paraffin embedded and 4μm sections were cut prior to haematoxylin and eosin staining.

Real Time Quantitative PCR

was performed using Taqman probes obtained from ABI for *Btbd12* (Mm01342405_m1). RNA was isolated from *Btbd12*$^{+/+}$ and *Btbd12*$^{-/-}$ using Trizol (Invitrogen) and reverse transcription was performed using random hexamers and SuperScript III(Invitrogen). All measurements were performed in triplicate and the relative amounts of cDNA were compared with Hprt (Mm00446968_m1) as a reference for total cDNA. Subsequently, the *Btbd12*$^{+/+}$ cDNA concentration was used for normalization.

LacZ staining

was performed on tissues which were removed and fixed in 4% paraformadehyde for 30 minutes. Tissues were then washed three times in PBS supplemented with 5 mM EGTA , 0.01% Deoxycholate, 0.02% NP-40 and 2 mM $MgCl_2$. Tissues were then incubated at 37°C for 6 hours in staining buffer (5 mM $K_3Fe(CN)_6$, 5 mM $K_4Fe(CN)_6$, 5 mM EGTA, 0.01% Deoxycholate, 0.02% NP-40, 2 mM $MgCl_2$, 1mg/mL bromo-chloro-indolyl-galactopyranoside) in the dark. Tissues were fixed again with 4% paraformaldehyde overnight at 4°C before being transferred to 30% glycerol in 70% ethanol for long-term storage.

TUNEL Assay

was performed using TACS 2 TdT Blue Label (Trevigen) following for the manufacturers instructions. DNaseI treatment was used a positive control.

Glucose tolerance

was assessed in mice fed on a High Fat Diet (Western RD, 829100, Special Diets Services) from 4 weeks old until mice reached 13 weeks. At 13 weeks mice were fasted overnight before a blood sample was taken and glucose measured using an Accu-Check Aviva (Roche). To perform intra-peritoneal glucose tolerance test (IP-GTT) mice were fasted for 16 – hours a bolus of glucose was administered intraperitoneally and blood glucose

concentration from tail vein was measured using Accu-Check Aviva (Roche) after 15, 30, 60 and 120 minutes.

Clinical chemistry

was performed on 15-week-old mice. Mice were terminally anaesthetized and blood collected from the retro-orbital sinus into lithium-heparin tubes. Plasma was immediately analyzed on an Olympus AU400 Analyzer.

Neurobehavioural and Sensory assessment

was performed. At 9 weeks Open field, grip strength and modified SHIRPA were performed as described previously [2627]. Startle response was assessed at 11 weeks and hot plate was performed at 12 weeks.

Occular assessement

was performed at 13 weeks using a Zeiss SL130 Slit –Lamp and a Heine Omega 500 Binocular Indirect Ophthalmoscope. Tropicamide was used to dilate pupil.

X-ray imaging

was performed at 14 weeks using a MX20 Imager (Flaxitron). Mice were anaesthetized with Ketamine(100mg/kg), Xylazine (10mg/kg), Antisedan (1mg/kg) combination.

Supplementary Material

Refer to Web version on PubMed Central for supplementary material.

Acknowledgments

We wish to thank L Neidernhofer for the kind gift of Ercc1 deficient and wildtype congenic murine embryonic fibroblasts. Fanca and Fancc deficient MEFs were obtained from the Fanconi Anaemia Research Fund Cell Repository, Oregon. We thank Amita Shortland for significant contributions in the planning of animal experiments. The authors would like to thank Martin Taylor for cloning of the murine Slx4 cDNA. We would also like to thank Theresa Langford, James Cruickshank, Annie Mead, Michael Brown, , Karen Robinson, Caroline Shepherd, Martin Reed, and Richard Berks for assistance in animal husbandry and handling. We would also thank Dr G Nemeth (Mediso Ltd.) for assistance with the CT methodology. DJA was supported by CR-UK and the Wellcome Trust. PHLG is supported by ATIP-CNRS, ARC and FRM grants.

REFERENCES

1. Ciccia A, McDonald N, West SC. Structural and functional relationships of the XPF/MUS81 family of proteins. Annu Rev Biochem. 2008; 77:259–87. [PubMed: 18518821]
2. Svendsen JM, Harper JW. GEN1/Yen1 and the SLX4 complex: Solutions to the problem of Holliday junction resolution. Genes Dev. 24:521–36. [PubMed: 20203129]
3. Coulon S, et al. Slx1-Slx4 are subunits of a structure-specific endonuclease that maintains ribosomal DNA in fission yeast. Mol Biol Cell. 2004; 15:71–80. [PubMed: 14528010]
4. Fricke WM, Brill SJ. Slx1-Slx4 is a second structure-specific endonuclease functionally redundant with Sgs1-Top3. Genes Dev. 2003; 17:1768–78. [PubMed: 12832395]
5. Fekairi S, et al. Human SLX4 is a Holliday junction resolvase subunit that binds multiple DNA repair/recombination endonucleases. Cell. 2009; 138:78–89. [PubMed: 19596236]
6. Svendsen JM, et al. Mammalian BTBD12/SLX4 assembles a Holliday junction resolvase and is required for DNA repair. Cell. 2009; 138:63–77. [PubMed: 19596235]
7. Munoz IM, et al. Coordination of structure-specific nucleases by human SLX4/BTBD12 is required for DNA repair. Mol Cell. 2009; 35:116–27. [PubMed: 19595721]

8. Flott S, et al. Phosphorylation of Slx4 by Mec1 and Tel1 regulates the single-strand annealing mode of DNA repair in budding yeast. Mol Cell Biol. 2007; 27:6433–45. [PubMed: 17636031]
9. Matsuoka S, et al. ATM and ATR substrate analysis reveals extensive protein networks responsive to DNA damage. Science. 2007; 316:1160–6. [PubMed: 17525332]
10. Cheng NC, et al. Mice with a targeted disruption of the Fanconi anemia homolog Fanca. Hum Mol Genet. 2000; 9:1805–11. [PubMed: 10915769]
11. Lu B, Bishop CE. Late onset of spermatogenesis and gain of fertility in POG-deficient mice indicate that POG is not necessary for the proliferation of spermatogonia. Biol Reprod. 2003; 69:161–8. [PubMed: 12606378]
12. Agoulnik AI, et al. A novel gene, Pog, is necessary for primordial germ cell proliferation in the mouse and underlies the germ cell deficient mutation, gcd. Hum Mol Genet. 2002; 11:3047–53. [PubMed: 12417526]
13. Houghtaling S, et al. Epithelial cancer in Fanconi anemia complementation group D2 (Fancd2) knockout mice. Genes Dev. 2003; 17:2021–35. [PubMed: 12893777]
14. Adams DJ, et al. BRCTx is a novel, highly conserved RAD18-interacting protein. Mol Cell Biol. 2005; 25:779–88. [PubMed: 15632077]
15. Patel KJ, Joenje H. Fanconi anemia and DNA replication repair. DNA Repair (Amst). 2007; 6:885–90. [PubMed: 17481966]
16. Zhang XY, et al. Xpf and not the Fanconi anaemia proteins or Rev3 accounts for the extreme resistance to cisplatin in Dictyostelium discoideum. PLoS Genet. 2009; 5:e1000645. [PubMed: 19763158]
17. Dendouga N, et al. Disruption of murine Mus81 increases genomic instability and DNA damage sensitivity but does not promote tumorigenesis. Mol Cell Biol. 2005; 25:7569–79. [PubMed: 16107704]
18. Gillio AP, Verlander PC, Batish SD, Giampietro PF, Auerbach AD. Phenotypic consequences of mutations in the Fanconi anemia FAC gene: an International Fanconi Anemia Registry study. Blood. 1997; 90:105–10. [PubMed: 9207444]
19. Hsia KT, et al. DNA repair gene Ercc1 is essential for normal spermatogenesis and oogenesis and for functional integrity of germ cell DNA in the mouse. Development. 2003; 130:369–78. [PubMed: 12466203]
20. Weeda G, et al. Disruption of mouse ERCC1 results in a novel repair syndrome with growth failure, nuclear abnormalities and senescence. Curr Biol. 1997; 7:427–39. [PubMed: 9197240]
21. McWhir J, Selfridge J, Harrison DJ, Squires S, Melton DW. Mice with DNA repair gene (ERCC-1) deficiency have elevated levels of p53, liver nuclear abnormalities and die before weaning. Nat Genet. 1993; 5:217–24. [PubMed: 8275084]
22. Selfridge J, Hsia KT, Redhead NJ, Melton DW. Correction of liver dysfunction in DNA repair-deficient mice with an ERCC1 transgene. Nucleic Acids Res. 2001; 29:4541–50. [PubMed: 11713303]
23. Lawrence NJ, Sacco JJ, Brownstein DG, Gillingwater TH, Melton DW. A neurological phenotype in mice with DNA repair gene Ercc1 deficiency. DNA Repair (Amst). 2008; 7:281–91. [PubMed: 18221731]
24. de Waard MC, et al. Age-related motor neuron degeneration in DNA repair-deficient Ercc1 mice. Acta Neuropathol. 120:461–75. [PubMed: 20602234]
25. Pace P, et al. FANCE: the link between Fanconi anaemia complex assembly and activity. EMBO J. 2002; 21:3414–3423. [PubMed: 12093742]
26. Hancock JM, et al. Mouse Phenotype Database Integration Consortium: integration [corrected] of mouse phenome data resources. Mamm Genome. 2007; 18:157–63. [PubMed: 17436037]
27. Masuya H, et al. Implementation of the modified-SHIRPA protocol for screening of dominant phenotypes in a large-scale ENU mutagenesis program. Mamm Genome. 2005; 16:829–37. [PubMed: 16284798]

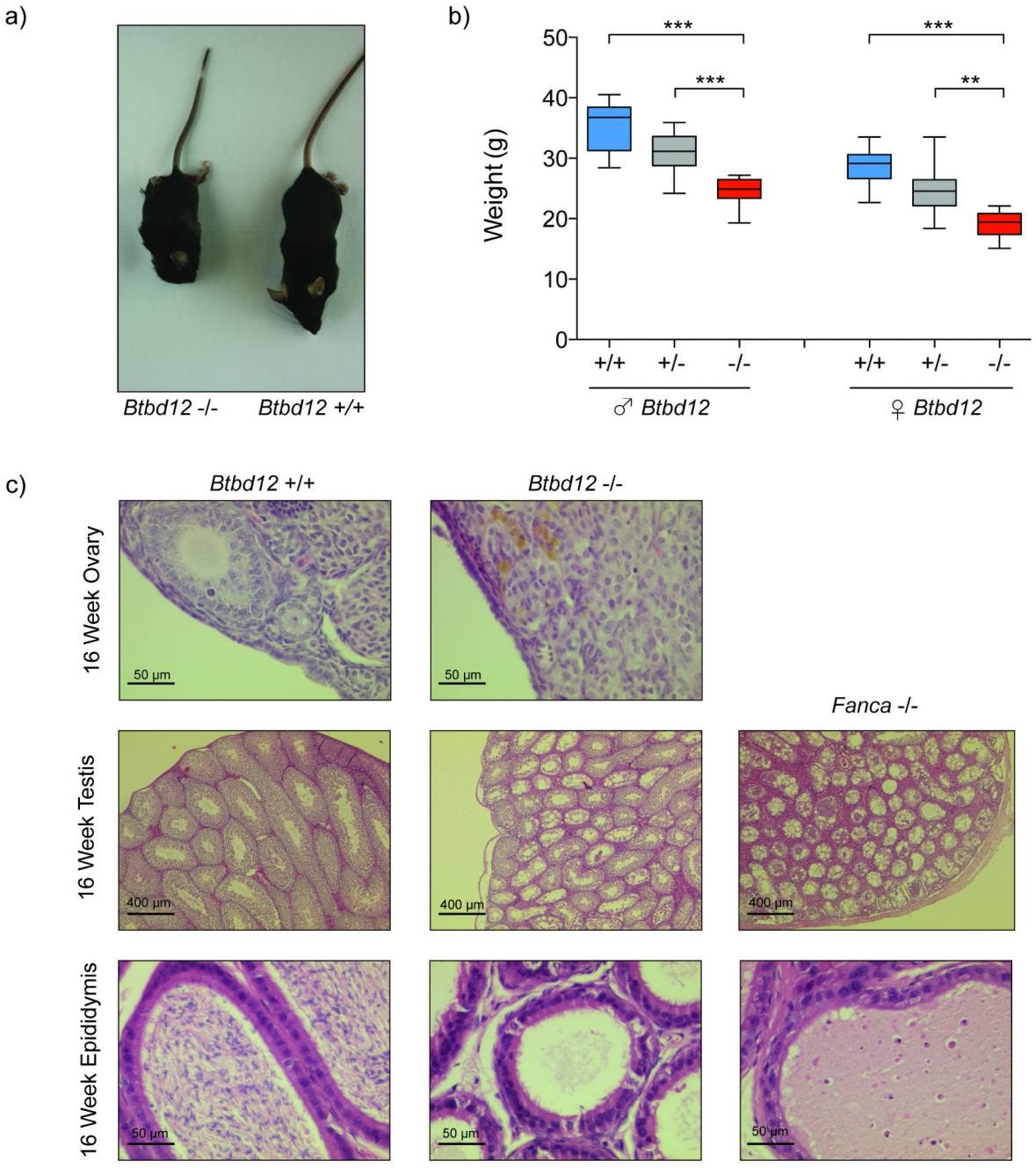

Figure 1. *Btbd12* deficiency results in growth retardation and compromised fertility

a) A representative image of *Btbd12*$^{+/+}$ and *Btbd12*$^{-/-}$ littermates at 7 weeks revealing obvious growth retardation. **b)** Weights of male and female *Btbd12*$^{+/+}$, *Btbd12*$^{+/-}$, and *Btbd12*$^{-/-}$ animals at 12 weeks confirming growth retardation of *Btbd12*$^{-/-}$ mice. (n=10 for each genotype, central line represents median, box interquartile range, whiskers 90th centiles, *** p<0.001, ** p<0.01.) **c)** Microscopic analysis of H&E stained sections of ovary (x400, scale bar 50μm), testis (x50, scale bar 400μm) and epididymis (x400, scale bar 50μm) from *Btbd12*$^{+/+}$, *Btbd12*$^{-/-}$ and *Fanca*$^{-/-}$ animals at 16 weeks. This revealed absence

Europe PMC Funders Author Manuscripts

of oocyte maturation in *Btbd12*$^{-/-}$ females, and similar pattern of impaired spermatogenesis in testis of *Btbd12*$^{-/-}$ and *Fanca*$^{-/-}$ mice with absence of spermatozoa from epididymis.

Europe PMC Funders Author Manuscripts

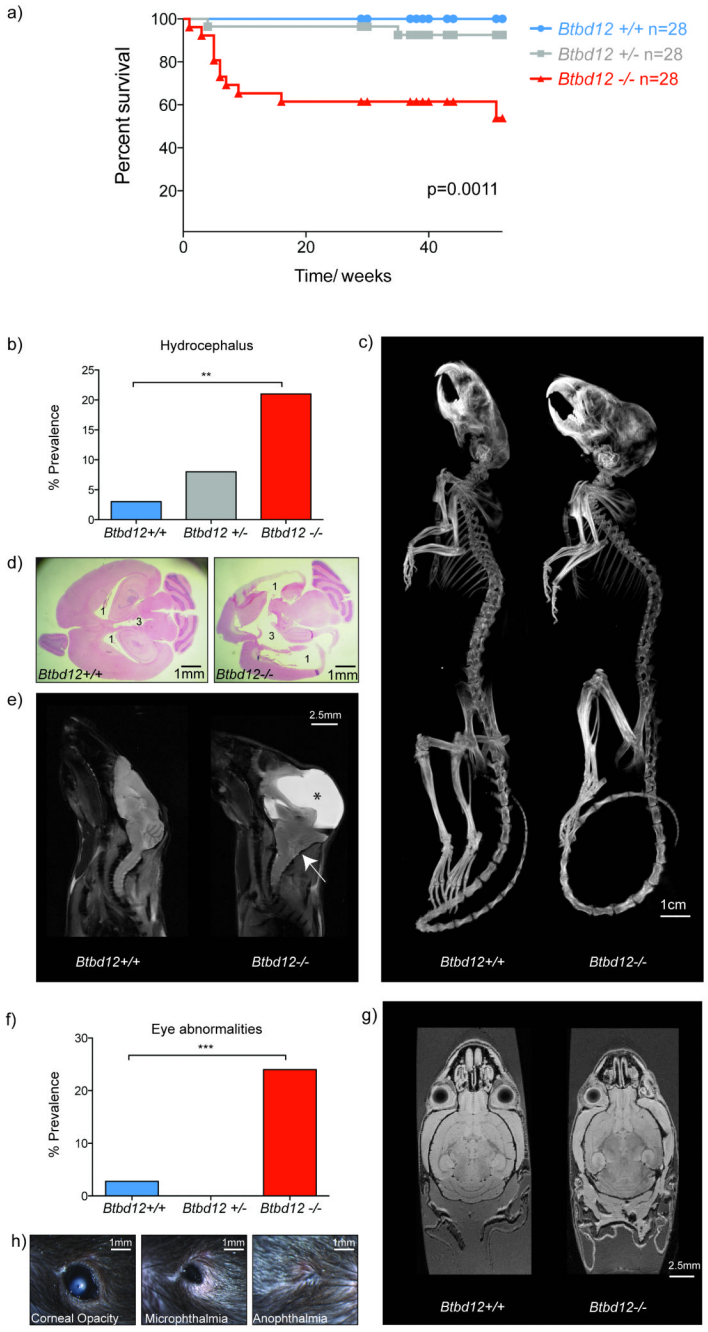

Figure 2. Some *Btbd12*$^{-/-}$ mice die prematurely and display brain and eye developmental defects

a) Kaplan-Meier survival curve for cohorts of *Btbd12*$^{+/+}$, *Btbd12*$^{+/-}$ and *Btbd12*$^{-/-}$ mice (n=28 per genotype, p=0.011), a sharp drop in survival is evident in the *Btbd12*$^{-/-}$ colony occurring within the first 3 months of life. **b)** An increased prevalence of hydrocephalus is observed among the cohort of *Btbd12*$^{-/-}$ mice. (**p=0.006, Fisher's exact test; *Btbd12*$^{+/+}$ n=3/72, *Btbd12*$^{+/-}$ n=13/163, *Btbd12*$^{-/-}$ n=10/48) **c)** High resolution X-ray CT of representative *Btbd12*$^{-/-}$ compared with littermate *Btbd12*$^{+/+}$ control, a obvious skull deformity is apparent in the *Btbd12*$^{-/-}$ mouse (scale bar 1cm). **d)** H&E sectioned hydrocephalic brain from a *Btbd12*$^{-/-}$ mouse showing dilatation of the lateral ventricles (1)

and rupture of the 3rd ventricle (3). (scale bar 1mm) **e)** High resolution MRI of a *Btbd12*$^{+/+}$ animal compared with a hydrocephalic *Btbd12*$^{-/-}$ mouse. The image shows a large hydrocephalus (*), arrowhead points to disrupted brainstem structure (scale bar 2.5mm). **f)** An increased prevalence of a spectrum of eye abnormalities is observed in *Btbd12*$^{-/-}$ mice (*** p=0.0008, Fisher's exact test; *Btbd12*$^{+/+}$ n=2/71, *Btbd12*$^{+/-}$ n=*0/163*, *Btbd12*$^{-/-}$ n=11/48) **g)** High resolution MRI of representative *Btbd12*$^{-/-}$ compared with wild type littermate showing unilateral anophthalmia (scale bar 2.5mm). **h)** Slit-lamp images revealing the spectrum of ocular abnormalities observed in the cohort of *Btbd12*$^{-/-}$ animals (scale bar 1mm). These abnormalities range from corneal opacity (left), to microphthalmia (center) and finally anophthalmia (right).

Europe PMC Funders Author Manuscripts

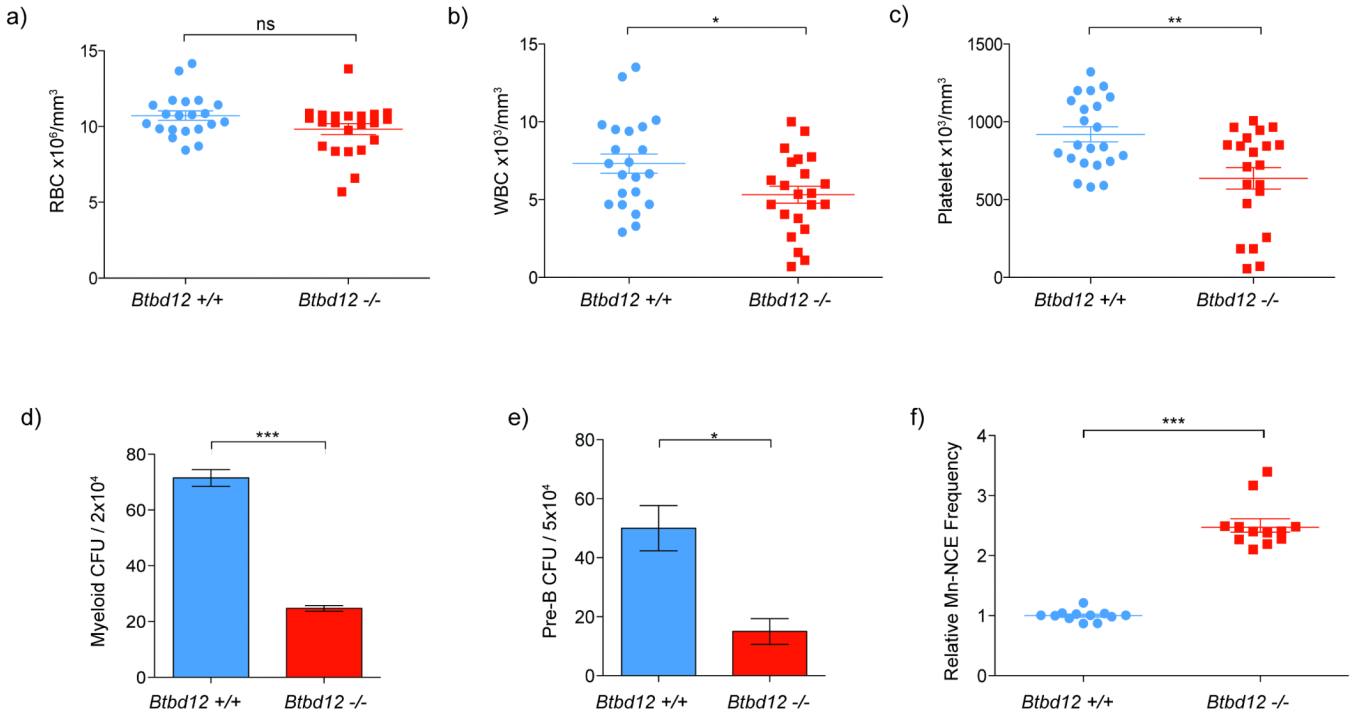

Figure 3. A proportion of *Btbd12*$^{-/-}$ mice develop blood cytopenias associated with genomic instability

Full blood count analysis of 4-12 weeks old *Btbd12*$^{-/-}$ with wild type littermates a-c (n=22 for each group) **a)** Peripheral blood erythrocyte concentration, ns; not significant p=0.0617 **b)** Peripheral white cell concentration, *p=0.0155 – note a sub-population of markedly leukopenic animals. **c)** Peripheral thrombocyte concentration, **p=0.0027 – note a sub-population of severely thrombocytopenic animals. (in a-c central line represents mean and error bars standard error of mean) **d)** Proficiency of *Btbd12*$^{+/+}$ and *Btbd12*$^{-/-}$ bone marrow progenitor cells to form myeloid colony forming units (CFU) from 2×10^4 nucleated bone marrow cells. Data obtained from the average of results obtained from 3 individual mice (***p<0.0001, bar represents mean of three independent experiments and error bars standard error of mean) **e)** Lymphoid linage was assessed through the ability of bone marrow cells to form Pre-B cell CFU per 5×10^4 bone marrow cells (average 3 independent mice, *p=0.017, bar represents mean of three independent experiments and error bars standard error of mean). **f)** Flow cytometric analysis revealing the frequency of micronucleated normochromic erythrocytes (Mn-NCE) in peripheral blood of unchallenged 16-week-old *Btbd12*$^{+/+}$ and *Btbd12*$^{-/-}$ mice (n=12 per genotype, ***p<0.0001, central line represents mean and error bars standard error of mean). Micronuclei are a marker for genomic instability.

Europe PMC Funders Author Manuscripts

Europe PMC Funders Author Manuscripts

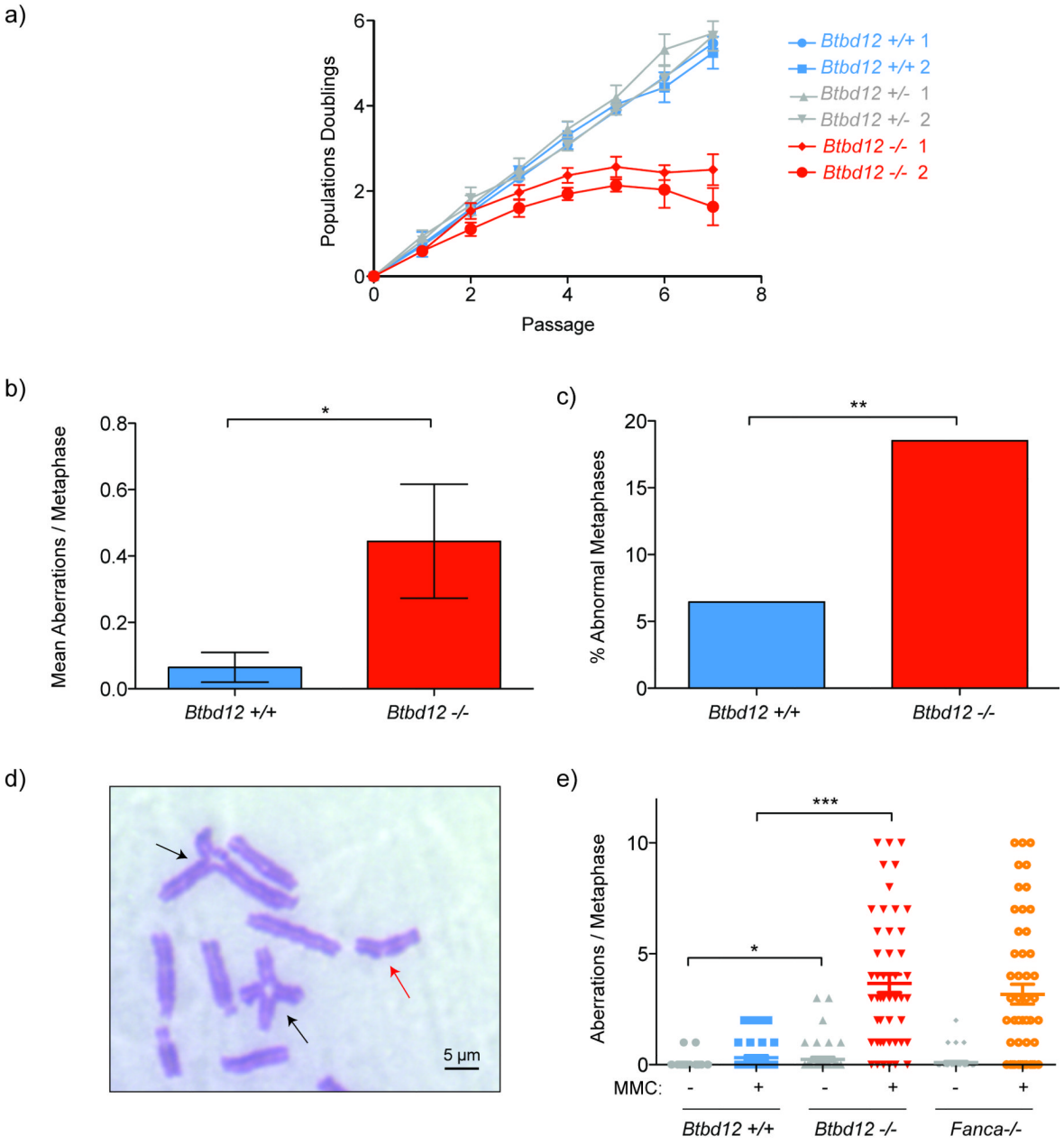

Figure 4. *Btbd12* deficient cells undergo premature replicative senescence exhibiting spontaneous and inducible chromosomal instability

a) Primary MEFs obtained from *Btbd12*$^{+/+}$, *Btbd12*$^{+/-}$, and *Btbd12*$^{-/-}$ embryos were grown in culture under normoxic conditions and monitored for population doubling. The *Btbd12*$^{-/-}$ MEF lines prematurely cease growing. Metaphases from early passage (P3) MEFs were prepared and individually imaged. Each metaphase was then scored blind for the presence of chromosome abnormalities revealing an increased **b)** number of aberrations per metaphase (* p = 0.0268, t-test; bar represents mean and error bars standard error of mean) and **c)** an increased frequency of abnormal metaphases (**p=0.0092, Fischers' exact test). **d)** Image of a single *Btbd12*$^{-/-}$ metaphase spread revealing chromosome aberrations similar to those seen in FA cells (black arrows - radial structures; red arrows - chromatid break, scale bar 5µm). **e)** Cells were exposed to MMC, metaphases from these cells were scored for

chromosome aberrations. MMC exposure leads to chromosomal instability in *Btbd12*$^{-/-}$ and *Fanca*$^{-/-}$ transformed MEFs (* p<0.05, **p<0.0001, t-test; central line represents mean and error bars standard error of mean)

Europe PMC Funders Author Manuscripts

Europe PMC Funders Author Manuscripts

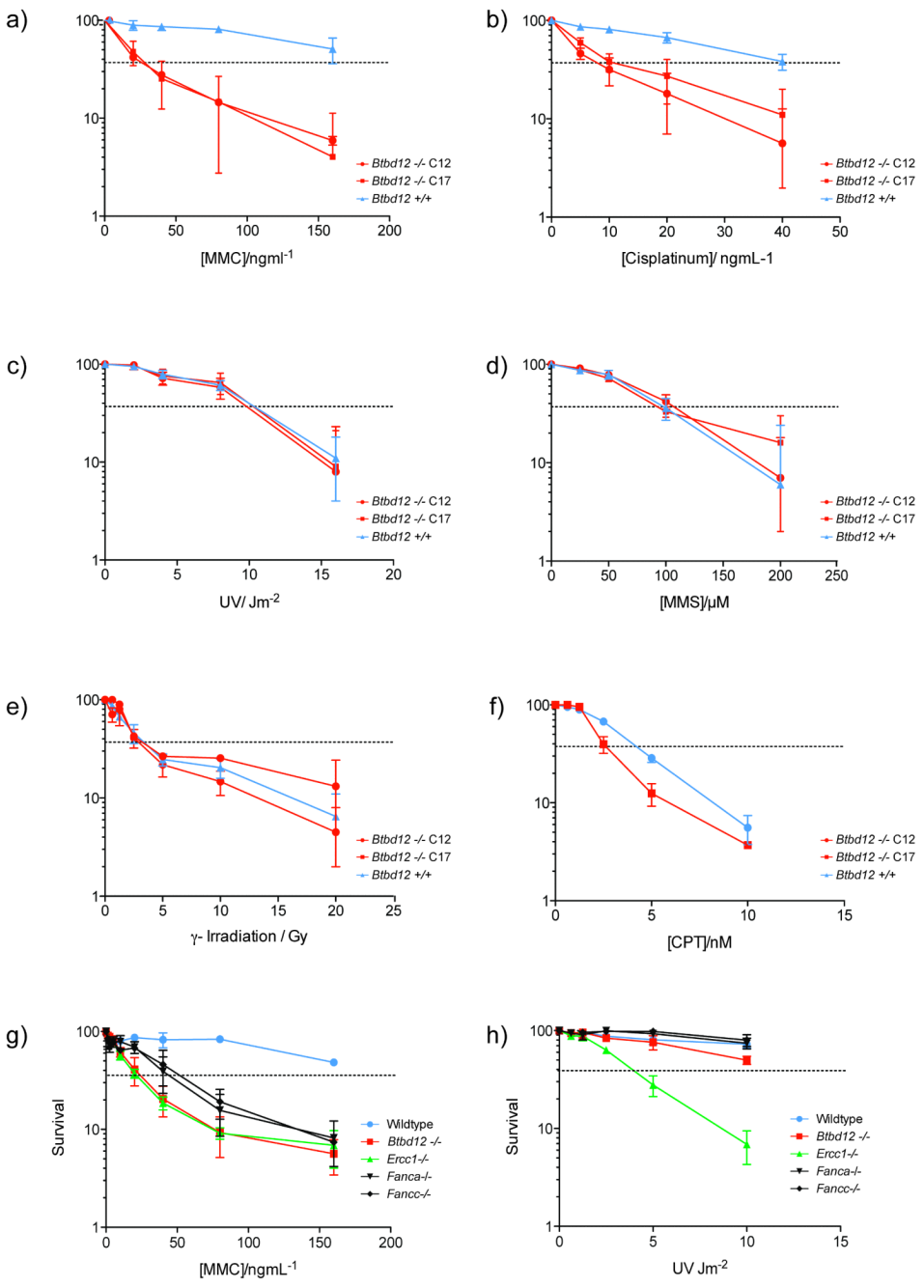

Figure 5. *Btbd12* deficient MEF are hypersensitive to DNA interstrand crosslinking agents

Two independent *Btbd12*$^{-/-}$ transformed MEF lines were compared with congenic wildtype transformed MEFs for cellular sensitivity to a range of mutagens by MTS cell viability assay. *Btbd12*$^{-/-}$ MEFs were extremely sensitivity to **a)** mitomycin C (MMC), **b)** cisplatinum, whilst they are not hypersensitive to **c)** UV irradiation, **d)** Methyl methanesulponate (MMS) or **e)** γ-irradiation. *Btbd12*$^{-/-}$ MEFs were mildly sensitive to **f)** camptothecin (CPT). The cellular sensitivity of *Btbd12*$^{-/-}$, *Ercc1*$^{-/-}$, *Fanca*$^{-/-}$ and *Fancc*$^{-/-}$ MEFs were compared next to each other to **g)** the DNA crosslinking agent MMC and **h)** UV

irradiation. Each point represents mean of three independent experiments, each carried out in triplicate, error bars represent standard error of the mean.

Europe PMC Funders Author Manuscripts

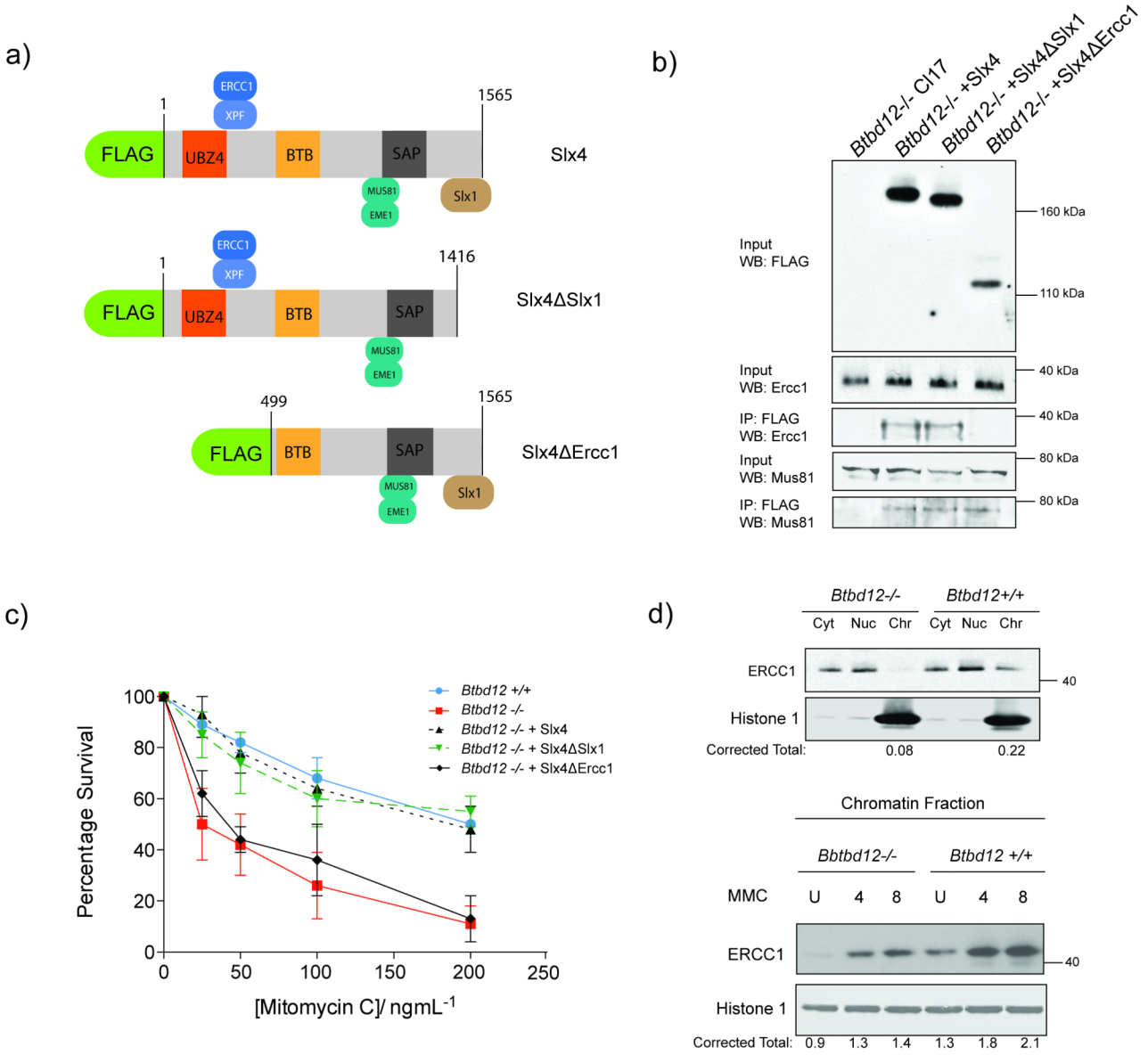

Figure 6. The interaction between Slx4 and Xpf-Ercc1 is required for crosslink repair

a) Cartoon representation of the Slx4 polypeptide, domain boundaries and interaction sites for the relevant SSEs (Xpf-Ercc1, Mus81-Eme1 and Slx1) are shown. Two deletion constructs that were predicted to disrupt the interaction with Slx1 (Slx4ΔSlx1) or the interaction with Xpf-Ercc1 (Slx4ΔErcc1) are described. **b)** Anti–FLAG Western blot showing the expression of FLAG-Slx4 and the truncations FLAG-Slx4ΔSlx1 and FLAG-Slx4ΔErcc1 in transfected *Btbd12*$^{-/-}$ tMEFs. FLAG IP were then Western blotted for Ercc1, the full length and FLAG-Slx4ΔSlx1 retain interaction to this SSE subcomponent whilst FLAG-Slx4 Ercc1 abolishes this. The IP was also blotted for Mus81 showing that all truncations interact with Mus81. **c)** MTS cell survival of *Btbd12*$^{-/-}$, *Btbd12*$^{-/-}$ + Slx4ΔErcc1 and *Btbd12*$^{-/-}$ + Slx4ΔSlx1 strains in response to MMC. Each point represents the mean of three independent experiments carried out in triplicate and error bars represent the standard error of the mean. **d)** Upper Panel: Sub-cellular fractionation followed by western blot for Ercc1 in cellular fractions without DNA damage (Cyt-cytoplasmic, Nuc-

nuclear, Chr-chromatin). A reduction of Ercc1 in the chromatin fraction is seen in the *Btbd12*$^{-/-}$ cell line without DNA damage Lower Panel: Western blot analysis of Ercc1 in the chromatin fractions of *Btbd12*$^{-/-}$ and *Btbd12*$^{+/+}$ tMEFs exposed to MMC (U-untreated, 4, 8). The accumulation of Ercc1 on chromatin is reduced after MMC treatment in *Btbd12*$^{-/-}$ cells.

Europe PMC Funders Author Manuscripts